NASA TECHNICAL MEMORANDUM

NASA TM X-3094

NASA TM X-3094

SOME ASPECTS OF FLOX-METHANE ROCKET ENGINE THROTTLING

by Daniel E. Sokolowski, Ned P. Hasnum, and Edwin J. Seigwarth

Lewis Research Center
Cleveland, Ohio 44135

NATIONAL AERONAUTICS AND SPACE ADMINISTRATION • WASHINGTON, D. C. • SEPTEMBER 1974

1. Report No. NASA TM X-3094	2. Government Accession No.	3. Recipient's Catalog No
4. Title and Subtitle SOME ASPECTS OF FLOX-METHANE ROCKET ENGINE THROTTLING		5. Report Date September 1974 6. Performing Organization Code
7. Author(s) Daniel E. Sokolowski, Ned P. Hannum, and Edwin J. Seigwarth		8. Performing Organization Report No. E-7911
9. Performing Organization Name and Address Lewis Research Center National Aeronautics and Space Administration Cleveland, Ohio 44135		10. Work Unit No. 502-24 11. Contract or Grant No.
12. Sponsoring Agency Name and Address National Aeronautics and Space Administration Washington, D.C. 20546		13. Type of Report and Period Covered Technical Memorandum 14. Sponsoring Agency Code
15. Supplementary Notes		

16. Abstract

A brief program was conducted to increase the technology for throttling a FLOX-methane rocket engine. Four injector designs and two chamber profiles were experimentally evaluated for structural integrity, combustion efficiency, and resistance to combustion instabilities. Vacuum thrust measurements were used as a primary measure of combustion efficiency. Stability rating to test the sensitivity of the injectors to high-frequency combustion was conducted, but not extensively. While chamber pressure was always monitored to check for the possible presence of such instability, the results are not presented. To map the boundary between stable operation and chugging instability, chamber pressure was throttled downward from 689.5 to 206.9 kN/m^2 abs (100 to 30 psia). Best operational results were obtained with an injector configuration having no hydraulic swirlers, a 0.00102-m (0.040-in.) recessed FLOX tube, and a nonflared exit in the methane annulus. This injector design exhibited stable combustion and good integrity of hardware, and it exceeded the design goal efficiency (88 percent) at the 10 to 1 throttled condition.

17. Key Words (Suggested by Author(s))	18. Distribution Statement
Combustion Engine throttling FLOX-methane	Unclassified - unlimited Category 28

19. Security Classif. (of this report)	20. Security Classif. (of this page)	21. No. of Pages	22. Price*
Unclassified	Unclassified	27	$3.25

* For sale by the National Technical Information Service, Springfield, Virginia 22151

SOME ASPECTS OF FLOX-METHANE ROCKET ENGINE THROTTLING

by Daniel E. Sokolowski, Ned P. Hannum, and Edwin J. Seigwarth

Lewis Research Center

SUMMARY

A brief program was conducted to increase the technology for throttling a FLOX-methane rocket engine. Four injector designs and two chamber profiles were experimentally evaluated for structural integrity, combustion efficiency, and resistance to combustion instabilities. Vacuum thrust measurements were used as a primary measure of combustion efficiency. Stability rating to test the sensitivity of the injectors to high-frequency combustion instability was conducted, but it was not extensive. While chamber pressure was always monitored to check for the possible presence of such instability, the results are not presented. To map the boundary between stable operation and chugging instability, chamber pressure was throttled downward from 689.5 to 206.9 kilonewtons per square meter absolute (100 to 30 psia). Best operational results were obtained with an injector configuration having no hydraulic swirlers, a 0.00102-meter (0.040-in.) recessed FLOX tube, and a nonflared exit in the methane annulus. This injector design exhibited stable combustion and good integrity of hardware, and it exceeded the design goal efficiency (88 percent) at the 10 to 1 throttled condition.

INTRODUCTION

The requirements of space storability (up to 2 yr), high specific impulse, high bulk density, and hypergolicity are desirable attributes of propellants for use in upper stage propulsion systems. The propellant combination FLOX-methane appears to satisfy these requirements. The NASA Lewis Research Center has been engaged in programs to advance the technology of rocket propulsion systems for use with this propellant combination. Mission studies made by both NASA and the aerospace industry indicate that a propulsion system for deep space missions should be designed to be pump-fed, have a regeneratively cooled tapered combustion chamber, deliver a nominal 22.24-kilonewton (kN) (5000-lb) thrust at a chamber pressure of 3448 kilonewtons per square meter absolute (kN/m^2 abs) (500 psia), and have a 10 to 1 throttling range capability (i.e., 22.24

to 2.224 kN (5000 to 500 lb) thrust).

In order to insure the feasibility of operating this propulsion system over a 10 to 1 throttling range, an in-house study was initiated to broaden the throttling technology with regard to (1) combustor performance characteristics, (2) materials compatibility and fabrication techniques, and (3) system operating experience with this propellant combination. Performance evaluation criteria include both combustion efficiency and stability.

This report contains some of the more significant results of the throttling investigation. Most of the results reported herein are experimental but also included are pertinent supporting analytical efforts. Efforts were primarily directed at improving the combustion efficiency and minimizing the incurrence of combustion instabilities by making injector design changes. Qualitative results relative to the materials used and fabrication techniques that are deemed important are also reported.

APPARATUS

Test Facility

Tests were conducted in a facility equipped with a propellant supply system for gaseous methane and liquid FLOX (82.6 percent fluorine, 17.4 percent oxygen by weight). A schematic diagram of the propellant flow systems and instrumentation locations is shown in figure 1. Pressure-regulated helium gas controlled the flow rate of the liquid FLOX, while a pressure regulator controlled the gaseous methane flow rate. FLOX was supplied from a tank immersed in a liquid nitrogen bath. This bath also thermally conditioned two turbine-type flowmeters and the oxidizer fire valve. Methane was delivered at ambient (294.4 K (70° F)) temperature. Nominal flow rates at full thrust for FLOX and methane were 4.795 and 0.912 kilogram per second (10.57 and 2.01 lbm/sec), respectively. A photograph of a thrust stand and a combustor is shown in figure 2.

Combustors

An experimental evaluation of the injectors was conducted using graphite-lined combustion chambers and nozzles. The combustor was nominally rated at 16.24 kilonewtons (3650 lbf) of thrust (sea level) for a chamber pressure of 3448 kN/m^2 abs (500 psia). Two chamber configurations were used during the test program. Figure 3 contains a schematic of a typical thrust chamber configuration along with a tabulation of the specific dimensions for each configuration tested. In general, the chamber configurations

were (1) a full taper from the injector to the nozzle throat and (2) a nominal 0.134-meter (5.26-in.) cylindrical section (constant area) followed by a taper to the nozzle throat. The nominal nozzle throat diameter was 0.067 meter (2.361 in.) for all chambers.

Injectors

Specific injector element configurations evaluated experimentally are shown in figure 4 with the actual dimensions listed. Injector A had 19 oxidizer tubes (elements) with all the fuel flowing through a porous faceplate. Three other injector configurations (B, C, and D) having 61 coaxial elements were designed and fabricated for throttling evaluation. Injectors B and D were tested both with and without swirl as indicated in figure 4. Other modifications to the basic injector configurations, such as nickel elements and faceplate attachment methods (see fig. 4), were also fabricated and evaluated. Photographs of the injectors are shown in figures 5 to 8. Figure 9 illustrates the three types of swirlers tested.

Instrumentation

The location of the instrumentation used in the evaluations is illustrated in figure 1. Unprocessed data signals were digitized and recorded at a central facility for subsequent computer reduction to engineering units. Quartz piezoelectric-type pressure transducers were used to determine the frequencies of combustion instability. These transducers were mounted in water-cooled jackets recessed approximately 0.0048 meter (3/16 in.) from the inner chamber wall. According to the manufacturer's specifications, the low-pass frequency response characteristic of the transducers as installed is flat to within 10 percent up to a frequency of 10 000 hertz and has a nominal undamped natural frequency of 34 000 hertz.

Strain-gage-type pressure transducers coupled to two pressure taps in the injector faceplate monitored the static chamber pressure. Flow rates of the gaseous methane were measured by one of two systems - depending on the magnitude of flow rate expected: (1) two venturies in series, or (2) two orifices in series. The flow rates of liquid FLOX were measured by two turbine-type flowmeters in series. Line and flowmeter sizes were dependent on the magnitude of the flow rates expected.

Oxidant injection temperature was measured with a platinum-resistance element. All other temperatures were measured with standard iron/constantan thermocouples.

Data Recording and Retrieval

An IBM 360 time-sharing computer system provided digital data recording and reduction services throughout the test program. This system recorded all instrumentation signals sent from the test facility and performed two functions. The data recording system converted primary data to engineering units for analysis immediately following each run, and later it reduced all data in a more exacting manner.

All instability data were recorded on magnetic tape at 1.524 meters per second (60 in./sec) and replayed at an 8 to 1 reduced speed for visual monitoring on an oscillograph and oscilloscope located in the facility control room.

PROCEDURE

Prior to the initial run of each test day, a calibration was made of the thrust load cells with the complete engine assembly in place on the thrust stand. Calibration data were averaged and corrected for drift, and the calibration slope was determined by a standard computer program.

The operational technique used during the chugging instability test series was to throttle the engine static chamber pressure downward from 689.5 to approximately 241.3 kN/m^2 abs (100 to 35 psia) by throttling the propellant flow rates. This was accomplished by venting helium gas from the FLOX cryogenic tank which was initially pressurized for a static chamber pressure of 689.5 kN/m^2 abs (100 psia). Gaseous methane flow rates were automatically controlled to maintain a constant oxidant to fuel ratio of 5.25. Limit switches automatically terminated the run when the static chamber pressure reached the low value of 241.3 kN/m^2 abs (35 psia).

A typical automatic sequence timer activated the data acquisition equipment, propellant line purges, and engine propellant valves in preselected order. Critical operational parameters, such as chamber pressure and propellant flow rates, were recorded on oscillographs in the control room as well as on the high-speed data acquisition equipment.

RESULTS AND DISCUSSION

A program was conducted to evaluate the operating characteristics of a rocket engine using high-energy, space storable propellants (FLOX-methane) while operating in a throttling mode. Specifically, program goal was to assess the deep throttling characteristics of a 22.24-kilonewton (5000-lb) thrust FLOX-methane engine while main-

taining (1) reasonably high combustion performance over the full throttling range - 98 percent at full thrust down to 88 percent at 1/10 thrust, (2) complete combustion stability, and (3) integrity of engine hardware, especially with the injector and chamber walls. Because of the extreme reactivity and high combustion temperature of these propellants, minor design changes significantly affected injector durability. Problems of this sort and their solutions are discussed.

Several potential problem areas were investigated to increase our knowledge of the overall operation of a typical 22.24-kilonewton (5000-lb) thrust FLOX-methane engine. The first problem area investigated involved determining the relation for the flow through the type of porous materials used for the injector faceplates. This included a simulation of the environment experienced during combustor operation. Data from these experiments permitted a better understanding of the fuel flow split requirements for the injector elements and faceplate cooling. Another area was an analytical assessment of the thermal decomposition characteristics of methane when subjected to highly elevated temperatures. The results of this study revealed possible problems with carbon plateout on the engine hardware and deviations in predicted fluid properties due to dissociation.

The results are mostly experimental and identify some of the design improvements necessary to maximize engine efficiency while minimizing the incurrence of combustion instability as well as hardware degradation or failure while throttling the engine. The results of the investigations have been categorized into specific sections on Combustion Efficiency, Stability, Fabrication, and Related Technology.

Combustion Efficiency

Combustion efficiency of a rocket combustor is determined by measured values of the propellant flow rates and the resultant total chamber pressure or thrust. For the type of chambers used in this study, where all or part of the chamber is tapered toward the nozzle, an analytical determination of total pressure loss is not as simple as that for constant area chambers. Consequently, combustion efficiency based on thrust is more representative of the actual engine performance for this case. Because vacuum thrust measurements were used, care was taken to minimize nozzle base area by scalloping the base flange and minimizing base pressures by using an exhaust diffuser.

One of the primary objectives of this study was to design and test a relatively simple injector which would provide combustion efficiencies of at least 98 and 88 percent at the extreme chamber pressures of 3448 and 344.8 kN/m^2 abs (500 and 50 psia), respectively. The following data illustrate the effects of some of the design changes made to improve overall injector performance. For this particular case, performance in-

cludes not only combustion efficiency but also combustion stability and qualitative effects on the injector face and chamber walls such as streaking and hot spots.

In order to make relative comparisons of the effects of combustor design changes on efficiency, data were obtained with a baseline injector design tested in combustion chambers having two different profiles. As shown in figures 4 and 6, the baseline injector design (injector B) had coaxial elements - FLOX in the tube surrounded by methane in the annulus, a 0.785-radian (45°) expansion angle at the annulus exit, a 0.0034-meter (0.135-in.) tube recess from the face-plane, no hydraulic swirlers in the oxidizer tubes, and the same constant areas for flowmetering in all elements. The combustion chamber profiles were either (1) fully tapered from an injector end diameter of 0.134 meter (5.26 in.) nominally to a nozzle throat diameter of 0.067 meter (2.63 in.) nominally or (2) a constant diameter of 0.134 meter (5.26 in.) for the first 0.127 meter (5 in.) from the injector face followed by a taper to the same throat diameter as before. The contraction ratio was approximately 4.0, while the expansion ratio was 1.2. Oxidant to fuel ratios were varied from 2.5 to 6.0, while chamber pressures ranged from 3448 to 344.8 kN/m^2 abs (500 to 50 psia).

Presented in figure 10 is combustion efficiency (based on measured thrust) as a function of oxidant to fuel ratio (O/F) for the previous design (injector B). In general, over the chamber pressure range of operation the efficiency decreased with increasing O/F. At chamber pressures of 3448 and 1724 kN/m^2 abs (500 and 250 psia) combustion efficiency data were obtained using both the fully tapered and the constant cross-sectional area/partially tapered combustion chamber. In figure 10 the solid line through the 3448 kN/m^2 abs (500 psia) data represents the mean value of the data for the fully tapered chamber. A comparison with similar data from the other chamber profile, as well as a comparison of the 1724 kN/m^2 abs (250 psia) data with both chamber profiles, shows an apparent decrease in efficiency when switching from a fully tapered to a constant area/partially tapered chamber profile. This effect also has been noted by other investigators. For example, reference 1 has experimental data showing such an effect and gives a possible explanation. Furthermore, the efficiency of injector B at the design mixture ratio of 5.25 slightly exceeds the combustion efficiency goal of 88 percent in the 10 to 1 throttled condition but falls 5 to 6 percent short of the 98 percent goal at full thrust.

In the initial design of injector B the flow area for metering the fuel in each element was the same for all elements, and the flow area for metering the oxidant in each element was the same for all elements. Normally this would yield a constant mass flux distribution across the face-plane. Water flow tests of the oxidizer elements qualitatively showed an uneven mass flux distribution in the outer row of elements. It was concluded from the cold flow tests that the injector O/F distribution was not constant. Therefore, the elements in the outer row were changed to smaller oxidizer metering

areas.

In an effort to increase the combustion efficiency hydraulic swirlers were added to the oxidizer tubes (ref. 2). The first swirler design, as shown in figure 9(a), had two holes - both tangentially located to impart a swirling vector to the oxidizer flow as it flows axially down the oxidizer tube. The sizing of these holes in each row of elements effected the previous change in the O/F distribution. The total metering area of the oxidizer orifices remained unchanged.

The first test using this swirler design in injector B was a catastrophic failure. Inspection of the damaged elements indicated mild to severe burning of the expansion section of the fuel sleeves. It was concluded that excessive swirl resulted in large oxidizer spray cone angles and therefore caused the damage due to oxidizer impingement. To reduce the oxidizer cone angle a new two-hole swirler was designed with one hole located tangentially and the other located axially (fig. 9(b)). Again, total oxidizer orifice metering areas remained unchanged. A new injector body using the modified swirler design was reidentified as injector C.

In figure 11 the combustion efficiency as a function of oxidant to fuel ratio data shows the effect of changing the propellant mass distribution across the face-plane and adding two-hole hydraulic swirlers to improve the combustion efficiency as compared with the previous injector design (injector B). At a chamber pressure of 3448 kN/m^2 abs (500 psia) the improvement was about 3 percent (at the design O/F) over injector B. It also should be noted that the mean value curve through the data as well as the curve for the data without swirlers shown in figure 11 is for a constant area/partially tapered chamber profile as shown in figure 3. An additional increase in combustion efficiency of 1 percent (at the design O/F) could be realized by using a fully tapered chamber.

Some erosive burning of the fuel sleeves occurred on localized portions of several injector elements during the previous tests using both the unswirled (for example, see fig. 6) and swirled designs. Because any positive effect on performance by using the annulus flare has yet to be proven in this study, consideration was directed to other possible fuel sleeve configurations and faceplate attachment techniques. The resulting design had the recess reduced to 0.00102 meter (0.040 inch), no annulus flare, and welded studs for attachment purposes. Flowmetering areas remained the same as before. This injector design was designated injector D.

Presented in figure 12(a) is a plot of combustion efficiency as a function of oxidant to fuel ratio data from injector D tests. In this design a three-hole swirler design (shown in fig. 9(c)) was used to increase performance as before and make the swirl exit cone more symmetrical than that from the two-hole design. Test results were contrary to expectations. Not only was the efficiency drastically lowered at the 10 to 1 throttled chamber pressure, about 11 percent below the goal of 88 percent, but more importantly low-frequency combustion instability (chugging) was experienced. The details of this

instability are discussed further in the Stability section.

In an effort to separate which injector design-parameter changes adversely affected the combustor's performance (efficiency and stability) most drastically, each swirler was replaced by a straight tube, nonswirl, flowmetering insert design having the same flow area as before. Shown in figure 12(b) is combustion efficiency as a function of oxidant to fuel ratio data for the unswirled injector D. The combustion efficiency produced by this injector at low chamber pressures increased to a value greater than those using the baseline design (injector B) as shown in figure 10. Furthermore, stability against chugging was greatly improved. This is explained more in the next section. Plans for additional tests at high chamber pressures were not executed due to failure of injector D at the end of the previous test sequence. This was caused by an interpropellant leak in the injector manifold. The predicted combustion efficiency at full thrust for this injector design (nonswirled injector D) was estimated to be at least equal to or better than injector B, based on the relatively high efficiency (90 percent) and stability results at throttled conditions. Normally, combustion efficiency measured during a chugging instability mode of engine operation is lower than that during stable operation. Therefore, data in figure 12 should be compared with data in figure 10 accordingly.

Stability

The investigation of the combustion stability of the various injector/chamber configurations studied at Lewis was concerned primarily with the possible incurrences of low-frequency instability (chugging) during normal engine operation. Chamber pressure was monitored on all tests to check for any presence of high-frequency instability (screaming) at the high chamber pressure levels (approximately 3448 kN/m^2 abs (500 psia)). There were not enough data to establish a stability rating - using the multiple-shot gun of reference 3 - at the high chamber pressures. To map the boundary between stable operation and chugging instability, the chamber pressure was throttled downward from 689.5 kN/m^2 (100 psia) to approximately 206.9 kN/m^2 abs (30 psia) by throttling the propellant flows. At some point during throttling, well defined chamber pressure oscillations indicated the presence of chugging instability.

Injector A was not evaluated in these tests. Stability tests using injectors B and C (see fig. 4) were conducted over a chamber pressure range from 3448 to 344.8 kN/m^2 abs (500 to 50 psia) with no incurrence of instabilities. Combustion efficiency data from these tests are presented in figures 10 and 11.

Stability tests using injector D (see fig. 4) with three-hole oxidizer swirlers unexpectedly incurred low-frequency instability at relatively high chamber pressures. As shown in figure 13(a) a stability boundary was established over a wide range of chamber

pressures and oxidant to fuel ratios. At the design O/F of 5.25 chugging occurred at a chamber pressure of 551.6 kN/m^2 abs (80 psia). The chugging cycle had a frequency of 125 hertz at this operating condition.

A previous discussion in the Combustion Efficiency section noted the low combustion efficiency and the chugging when using swirlers in injector D. Eliminating the swirlers not only appeared to improve the efficiency at low chamber pressures (see fig. 12(b)) but greatly increased stable operating limits. Presented in figure 13(b) is the chamber pressure as a function of the oxidant to fuel ratio for the unswirled injector D. The location of the stability boundary relative to the superimposed boundary from figure 13(a) (swirled design) shows a marked improvement in stability. No chugging was experienced was at the design O/F of 5.25. The chugging that was experienced was at chamber pressures below 310.3 kN/m^2 abs (45 psia) and in an off-design O/F range. The measured chugging frequency ranged between 36 and 59 hertz as shown by the lower curve in figure 13(b).

Since stability against chugging is often discussed in terms of the injector pressure drop to chamber pressure ratios for the fuel and oxidizer, pertinent data from the stability tests presented in figure 13(a) were used to obtain a different form of stability map. Because of the relatively small range in values of the two ratios over that portion of the stability boundary determined, a plot of actual data points exhibited enough scatter to make any mean value line determination very difficult. The scatter can be attributed not only to experimental measurement errors but also to slight variations in chamber pressure and O/F from one test to another. Consequently, a graphic smoothing process was used to find mean values of the experimentally determined chugging frequency, propellant flow rates, fuel density, and injector pressure drops along the stability boundary in figure 13(a). The resulting stability boundary expressed as a function of the fuel and oxidizer injector pressure drop to chamber pressure ratios is presented in figure 14.

Fabrication

The criteria for designing the injectors were a compromise between accepted flight-weight practices and more versatile research hardware concepts. Methods of fabrication and installation sometimes had to be modified from the baseline design following failures not attributed to hardware design faults. The following discussion highlights some of the observed behavior of the hardware, especially with regard to use with the FLOX-methane propellant combination.

Removable dome. - Because of anticipated changes to the oxidizer tube inlets, easy access to the oxidizer manifold was necessary to reduce the time between configurations. Previous experiences with this design concept in oxygen systems indicated that oxidizer dome pressures up to 7989 kN/m^2 abs (1100 psia) could be tested without failures. This was made possible by using Teflon coated metal O-rings, high-strength bolts, and re-

torquing the bolts after the first pressure and thermal cycle. The possibility of contamination when the dome was opened seemed to be countered by the improved ability to clean the exposed surfaces. Confidence in using this design was verified by the successful FLOX-methane tests.

Faceplate attachment. - Selection of the method for faceplate attachment followed a Lewis ground rule requiring minimal relative motion between the faceplate and the coaxial propellant elements. The reason for this is discussed in the next section (Element design). For a reasonable faceplate thickness, approximately 0.0127 meter (0.5 in.), materials used for transpiration cooling cannot be supported adequately around only the periphery without incurring warpage. Techniques for further support were narrowed to using support posts. The concern with using support posts is in cooling the hot-gas side. This side may have either a weld or screw head, neither of which are simple to cool. For the tube supports the desirable annular pattern of fuel flow dictates using some form of sleeve between the tube and faceplate to maintain the annular gap and concentricity while offering support. The choices include welding, with again the inherent cooling problem and flaring the sleeve on the chamber side, thereby allowing leakage of fuel coolant around the flare. Based on an evaluation of all possible design configurations, posts were selected as the best configuration for use in this investigation. Figures 4 to 8 show the designs considered.

Element design. - Experience with coaxial elements has shown that annulus concentricity is important in preventing chamber wall streaking. Fuel sleeves were used to maintain concentricity as well as to provide a possible technique for faceplate attachment. Because the injectors were for research, it was desirable to make the faceplates removable. The initial injector design and fabrication steps called for first threading the fuel sleeves onto the oxidizer tubes, locating the faceplate in place, and then flaring the sleeves. Faceplate removal was accomplished by machining the flares; thus, reinstallation of a faceplate required new fuel sleeves.

Two problems were discovered with this design. First, normal tolerance on the threads were not adequate to prevent cocking of a sleeve with respect to a tube unless the top of a sleeve was bottomed against a shoulder at the base of the tube and second, the procedure for locating the oxidizer tubes for brazing allowed some variation in the axial position of the shoulder at the lower end of the sleeve (see fig. 4). Consequently, the faceplate could not be uniformly and rigidly secured to each tube's sleeve assembly after flaring. Also, the flared sleeve method of fabrication required some tube recess and thus limited the option of using smaller tube recess depths. While welded support posts allow rigid attachment of the faceplate, care had to be exercised to prevent the initially shouldered sleeves from unscrewing due to vibrations and thereby causing a cocked sleeve condition. A small weld or conically shaped key (produced by a punch), such as shown in figures 6 and 7, between the sleeve and faceplate prevented unscrewing.

Flightweight injector bodies and oxidizer tubes have been fabricated in one piece by intricate milling operations. For research injectors a less expensive technique was employed. In hydrogen-oxygen in-house tests at Lewis most of the injectors had the tubes brazed to the injector body. Common practice has been to provide a clearance of an interference fit to 7.62×10^{-5} meter (0.003 in.) between the tube and the injector body so as to ensure capillary flow of the braze material. There was concern that this brazing process might leave minute surface inclusions in the braze material that could not be cleaned adequately for use in a flourine environment. However, this technique was successful in the subject injector fabrication used in the present FLOX-methane tests.

Fuel sleeves were made from both 304 stainless steel and nickel. Each worked satisfactorily in tests where no oxidizer impinged directly on the sleeve tips. The higher thermal conductivity of the nickel was not necessary when no impingement occurred and was an inadequate solution when impingement did occur. It was concluded that no material will withstand direct impingement of a fluorinated oxidizer.

Oxidizer injection differential pressure and the amount of swirl were controlled by using brass inserts (shown in fig. 9) at the tube inlets. The technique of using removable inserts provided versatility of operation. Two problems were encountered as a result of this design. The plan was to use a press fit as the only method of attachment. For the first set tested the insert side walls were only 1.78×10^{-4} meter (0.007 in.) thick. When they were tapped into place the walls collapsed, thereby causing random flow variations as well as potential cleaning problems. The problem was eliminated by increasing the tube wall thickness to 6.1×10^{-4} meter (0.024 in.). A second minor fabrication problem was that of keeping the inserts in place. Postrun inspections revealed that some inserts were pushed back into the injector body until they were restrained by the oxidizer dome. Because the inserts could not come out completely, there was no apparent adverse effect on oxidizer flow.

Transducer modifications. - In earlier unreported Lewis tests with FLOX-methane, failures of the water cooled, helium bleed jackets for the quartz pressure transducers resulted soon after establishing steady-state operating conditions. These failures resulted in inadequate measurement of possible high-frequency chamber pressure oscillations. Then, as in the previous tests, the transducers were installed in thick heat-sink chambers (i.e., graphite lined). Analysis of the transducer failures indicated that there was adequate cooling of the tip of the transducer under normal use but that radiant heat addition from the chamber surrounding the jacket exceeded the design limits of the transducer assembly. Consequently, the transducer jackets were coated on the sides with rokide Z, a white zirconium oxide coating which can reflect radiant heat as well as provide insulation. As an added precaution, the transducer jacket face was recessed approximately 0.0048 meter (3/16 in.). After making these modifications, no further failures occurred.

Related Technology

The injector design concept used in this series of experiments has had extensive test experience in hydrogen-oxygen combustors such as the RL-10 and M-1 (refs. 4 and 5). For the faceplate material a sintered composite of woven wire mesh of stainless steel (Rigimesh) was used. Because this material has a porous structure, a part of the gaseous fuel in the fuel manifold can be injected into the combustion chamber in a diffuse manner. This process creates a protective boundary layer between the injector face and combustion field which acts to keep the faceplate relatively cool.

Since the fuel manifold feeds the fuel annuli of the injector elements as well as the flow through the faceplate material, establishment of a relation of flow rate against pressure drop for the wire mesh is desirable. This is necessary in order to know the fuel flow-split needed to make calculations of the fuel injection velocities. Manufacturers of the wire mesh material normally characterize the degree of porosity by stating the volumetric rate of flow of ambient air through a 0.093 square meter (1 ft^2) section at a specific pressure drop. When used near a high-temperature region, such as a combustion field, serious doubts arise regarding the validity of the manufacturer's flow relation. Uncertainties are due to the effects of heat transferred back into the porous faceplate. These effects may be exhibited as changed density and viscosity of fluid flowing through the faceplate, temperature and pressure gradients in the axial direction through the faceplate, and pore size changes of the material due to expansion and contraction.

To establish a flow relation for the type of mesh used and the operating conditions experienced in these experiments, tests were conducted using an injector with 19 oxidizer tubes (injector A) and all fuel injected through a wire mesh faceplate (see fig. 5). The manufacturer characterized the material as being able to pass 0.142 cubic meter per second (300 standard ft^3/min) of ambient air at a pressure drop of 137.9 kN/m^2 (20 $lb/in.^2$). This was designated Rigimesh II. The material surface area was 0.0124 square meter (19.15 $in.^2$). Figure 15 shows the flow rate as a function of pressure drop data for methane being burned at various chamber pressures for the Rigimesh II as well as another candidate porosity designated Rigimesh I.

In general, the flow behavior followed the usual square law for incompressible fluid flow. Since no S-shaped deviation (ref. 6) was found in the flow characteristics of figure 15, an implied result was that no temperature gradient existed through the faceplate. Besides allowing flow predictability, this result also indicated no adverse stress existed which could cause faceplate warpage. The Rigimesh II data presented in figure 15 were correlated by

$$\dot{\omega} = 0.001\, A\sqrt{\rho\, \Delta P}$$

where for the type of wire mesh stated previously, $\dot{\omega}$ is the methane flow rate through the mesh, ρ the methane density in the manifold, ΔP the pressure drop across the faceplate, and A the surface area of the mesh. The lowest flow rate per unit surface area tested was approximately 9.737 kilograms per square meter per second (0.01385 lb_m/ $in.^2$-sec). Perhaps at lower fluid flux values nonlinear effects due to heat transfer may be experienced.

For this investigation the physical properties of methane were obtained initially from a literature search of experimental data (for example, see ref. 7). Later, a computer subroutine called GASP (ref. 8) was used and found to be in excellent agreement with the experimental data. It was not only more versatile in application (has properties for eight fluids) but more complete in scope and range.

In a typical propellant flow cycle as envisioned for an advanced propulsion system design, the temperature of methane could reach as high as 1000 K (1800° R). Since a GASP subroutine only extends to 600 K (1080° R), additional methane property data were required. Another literature search yielded several bibliographies; for the 0 to 300 K (0° to 540° R) temperature range see reference 9, and for above 300 K (540° R) see reference 10. Unfortunately, in the extended temperature (1000 K (1800° R)) region of operation thermal decomposition of the methane does occur with the resultant solid carbon being formed. This result creates two problem areas. The first problem is the plating of carbon onto such hardware as heat exchangers, gas generators, turbines, etc., and onto coolant flow passages of the rocket combustion chamber and nozzle. This plating may cause possible restrictions of flows as well as possible wall temperature increases which would be due to increased thermal resistance on the coolant side. The second problem is due to the theoretically unpredictable deviations in fluid properties due to the dissociative process.

To gain insight into the severity of the dissociation problem, a brief theoretical study was made of the amount of decomposition after an " infinite" time of reaction. The methods used for this study are detailed in reference 11. Figure 16 shows the amount of graphite dissociated from methane as a function of temperature at several pressures. Some of the results found in reference 12 substantiate these findings. Results from this brief theoretical study for a nonflowing system indicate that the percent of mass that will plate-out is more severe at low pressures (in a constant temperature system).

The process of dissociation is not only a function of pressure and temperature but also is time dependent. An expected decomposition history is presented in figure 17. While the time-dependent decomposition is more pertinent to an engine throttling program, present knowledge is very limited in this "grey" region. Because of the many unknowns in the kinetic reaction rates, a theoretical prediction program seems impossible. Consequently, an experimental study is suggested to determine an empirical relation for the time-dependent thermal decomposition of methane.

SUMMARY OF RESULTS

A program was conducted to broaden the technological base with regard to the throttling limitations of a 22.24-kilonewton (5000-lb) thrust FLOX-methane rocket engine. Several injector designs and combustion chamber profiles were experimentally evaluated in an effort to achieve a good balance between structural integrity, high combustion efficiency, and resistance to combustion instabilities. Vacuum thrust measurements were used as a measure of combustion efficiency. No extensive injector stability rating was done at the high chamber pressure levels; however, pressure was monitored to check for any presence of high-frequency combustion instability. To map and establish a boundary between stable operation and chugging instability, chamber pressure was throttled downward from 689.5 to 206.9 kN/m^2 abs (100 to 30 psia). Some of the pertinent results obtained from this investigation are as follows:

1. The combustion efficiency showed an apparent decrease (of less than 2 percent) when the combustion chamber was changed from fully tapered to a constant area/partially tapered profile.

2. An increase of 3 percent in combustion efficiency was obtained by adding two-hole hydraulic swirlers (one hole tangentially located and one hole axially located) to an injector element design having a 0.0034 meter (0.135 in.) recessed FLOX tube and a 0.785 radian (45°) flared exit in the methane annulus. This design was stable with regard to chugging instability but seemed prone to random hotspots and burnouts of the annulus sleeves.

3. The best performance was obtained with an injector having no hydraulic swirlers, a 0.00102-meter (0.040-in.) recessed FLOX tube and no flared exit in the methane annulus. While exhibiting good hardware integrity, this injector design seemed very stable, especially with regard to chugging, and exceeded the design goal combustion efficiency of 88 percent at the 10 to 1 throttled condition. While no full thrust data were obtained, this injector (D) was felt to be at least equal to or better than the previous injector designs (B and C). With a three-hole swirler installed in each injector element of injector D, combustion efficiency was lowered drastically and chugging was experienced at the design operating condition.

Lewis Research Center,
National Aeronautics and Space Administration,
Cleveland, Ohio, May 14, 1974,
502-24.

REFERENCES

1. Wanhainen, John P.; Feiler, Charles E.; and Morgan, C. Joe: Effect of Chamber Pressure, Flow per Element, and Contraction Ratio on Acoustic-Mode Instability in Hydrogen-Oxygen Rockets. NASA TN D-4733, 1968.

2. Burry, R. V.: Space Storable Engine Characterization. R-7879, Rocketdyne (NASA CR-72559), 1970.

3. Sokolowski, Daniel E.: Improved Multiple-Shot Gun for Use as a Combustion Stability Rating Device. NASA TM X-2792, 1973.

4. Wanhainen, John P.; Antl, Robert J.; Hannum, Ned P.; and Mansour, Ali H.: Throttling Characteristics of a Hydrogen-Oxygen, Regeneratively Cooled, Pump-Fed Rocket Engine. NASA TM X-1043, 1964.

5. Pankhoff, Walter F.; Johnsen, Irving A.; Conrad, E. William; and Tomazic, William A.: M-1 Injector Development - Philosophy and Implementation. NASA TN D-4730, 1968.

6. Conrad, E. William; Wanhainen, John P.; and Curley, Jerome K.: Cooled Baffle Development for M-1 Engine Using a Subscale Rocket Engine. NASA TM X-1267, 1966.

7. Tester, H.E.: Methane. Thermodynamic Functions of Gases - Vol. 3. F. Din, ed., Butterworths Scientific Publications (London) 1961, pp. 1-71.

8. Hendricks, R.C.; Baron, A.; Peller, I.; and Pew, K.J.: GASP - A Properties Package for Eight Fluids - Helium, Methane, Neon, Nitrogen, Carbon Monoxide, Oxygen, Argon, Carbon Dioxide. Paper presented at XIII International Congress of Refrigeration. NAS-NRC, Washington, D. C., Aug. 27-Sept. 3, 1971.

9. Hall, L.A.: A Bibliography of Thermophysical Properties of Methane From 0 to 300° K. NBS-TN-367, National Bureau of Standards (NASA CR-95219), 1968.

10. Moore, R.T.; Harrison, R.H.; and Douslin, D.R.: Methane: Bibliography of the Thermodynamic and Transport Properties Above 300° K. BM-14-69, Bureau of Mines (PB-186243), 1969.

11. Zeleznik, Frank J.; and Gordon, Sanford: Calculation of Complex Chemical Equilibria. Indus. Eng. Chem., vol. 60, no. 6, June 1968, pp. 27-57.

12. Pugmire, T. Kent; Shaw, Robert; and Enos, George R.: Applied Resistojet Technology. J. Spacecraft, vol. 8, no. 1, Jan. 1971, pp. 63-68.

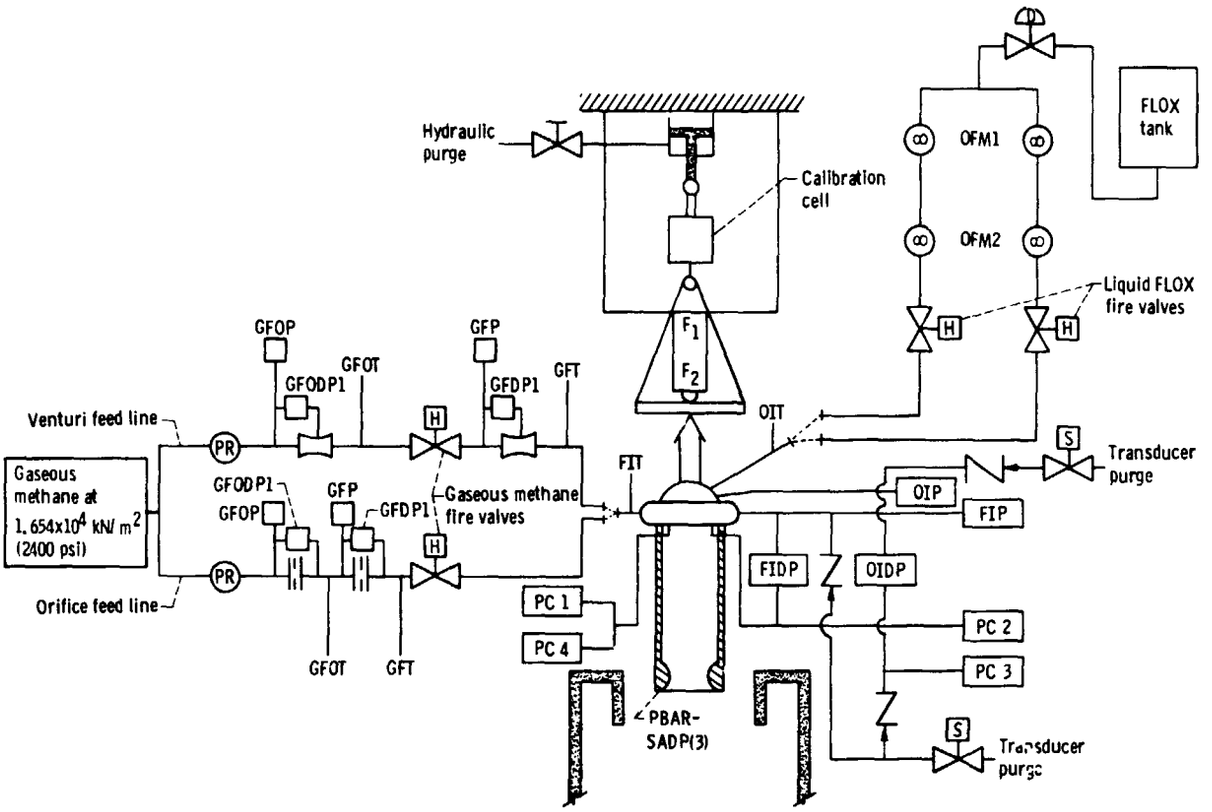

Symbol	Description	Instrumentation
GFOP	Gaseous fuel orifice pressure 1	Strain-gage transducer
GFODP1	Gaseous fuel orifice differential pressure 1	
GFP	Gaseous fuel orifice pressure 2	
GFDP2	Gaseous fuel orifice differential pressure 2	
PC1	Static chamber pressure 1	
PC2	Static chamber pressure 2	
PC3	Static chamber pressure 3	
PC4	Static chamber pressure 4	
FIP	Fuel injection pressure	
OIP	Oxidizer injection pressure	
FIDP	Fuel injection differential pressure	
OIDP	Oxidizer injection differential pressure	

Symbol	Description	Instrumentation
GFOT	Gaseous fuel orifice temperature 1	Iron-constantan
GFT	Gaseous fuel orifice temperature 2	
FIT	Fuel injection temperature	
OIT	Oxidizer injection temperature	
OFM1	Oxidizer flowmeter 1	Turbine
OFM2	Oxidizer flowmeter 2	Turbine
PR	Pressure regulator	-------
F1	Load cell	-------
F2	Load cell	-------
PBAR	Atmospheric pressure	-------
SADP(3)	Diffuser pressures(3)	Strain-gage transducer
-----	----------	----------
-------	----------	----------

Figure 1. - Schematic diagram of propellant flow systems and instrumentation locations.

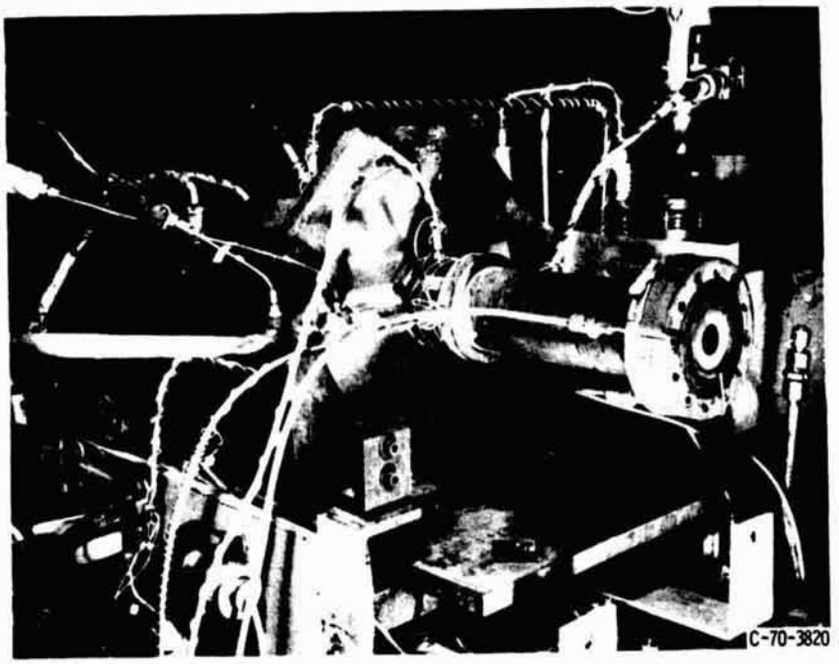

Figure 2. - Thrust stand with combustor.

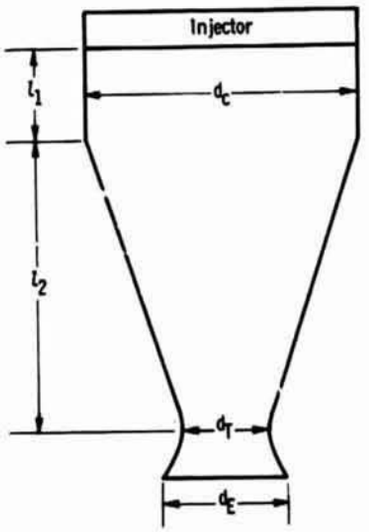

Chamber configuration	l_1, m(in.)	l_2, m(in.)	d_c, m(in.)	d_T, m(in.)	d_E, m(in.)
A	0.0(0.0)	0.152(6.0)	0.134(5.262)	0.067(2.631)	0.073(2.882)
B	.127(5.0)	.025(1.0)	.134(5.262)	.067(2.631)	.073(2.882)

Figure 3. - Chamber configuration detail.

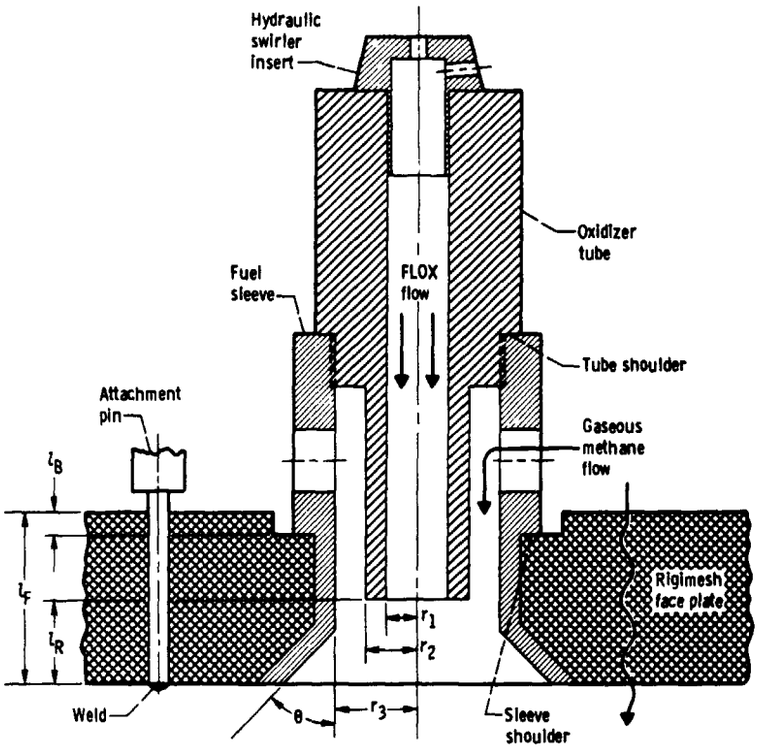

Injector	r_1, m	r_2, m	r_3, m	θ, radian	l_R, m	l_F, m	Without swirlers	With two-hole swirlers	With three-hole swirlers	Swirler axially located		Swirler tangentially located			With nickel elements	With faceplate attachment
										Hole diameter, m		Number of holes	Hole diameter, m			
										Three inner rows	One outer row		Inner row	Outer row		
A	0.0034	0.0034	0.0034	0	0	0.0079	x	---	---	------	------	---	------	------	---	---
B	.0014	.0018	.0020	.785	.0034		x	x	---	------	------	2	0.0008	0.0007	---	---
C	.0014	.0018	.0020	.785	.0034		---	x	---	0.0009	0.0008	1	.0009	.0008	x	---
D	.0014	.0018	.0020	0	.0010		x	---	x	.0011	.0009	2	.0007	.0007	---	x

Figure 4. - Injector element design and dimensions. (All injectors had 61 elements except injector A which had 19.)

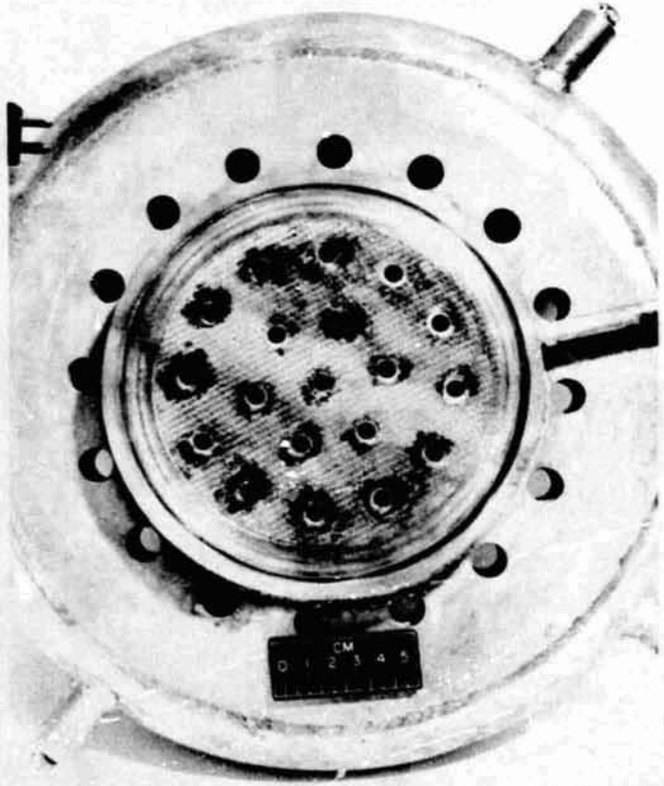

C-71-783

Figure 5. - Injector A (19 elements).

C-71-1896

Figure 6. - Injector B (61 elements).

C-71-2880

Figure 7. - Injector C (60 elements).

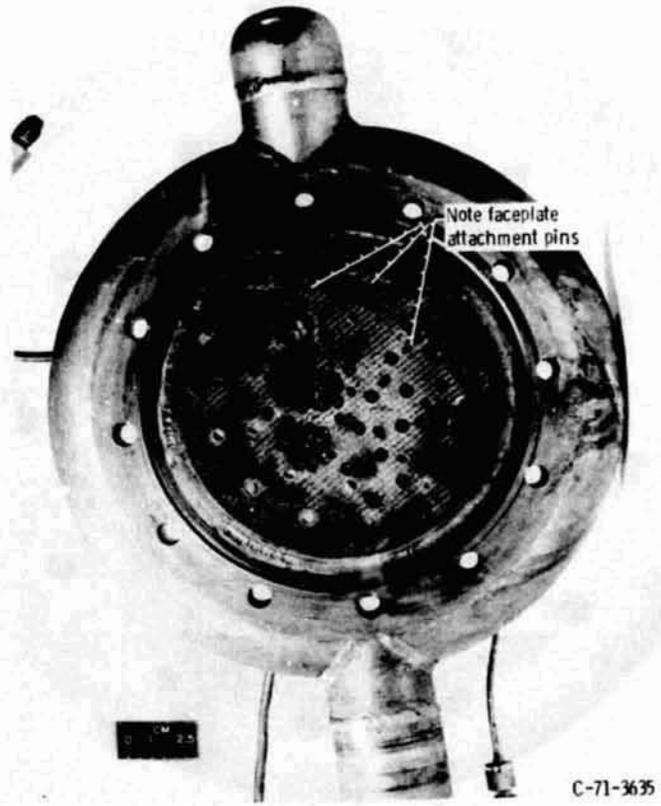

C-71-3635

Figure 8. - Injector D (61 elements).

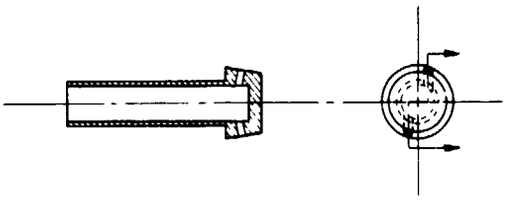

(a) Two-hole swirler. Swirler holes tangentially located; used on injector B.

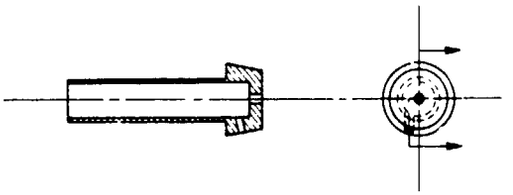

(b) Two-hole swirler. Swirler holes located tangentially and axially; used on injector C.

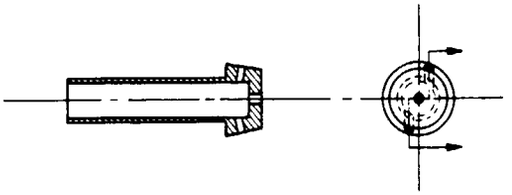

(c) Three-hole swirler. Two swirler holes located tangentially and one axially; used on injector D.

Figure 9. - Hydraulic swirler designs.

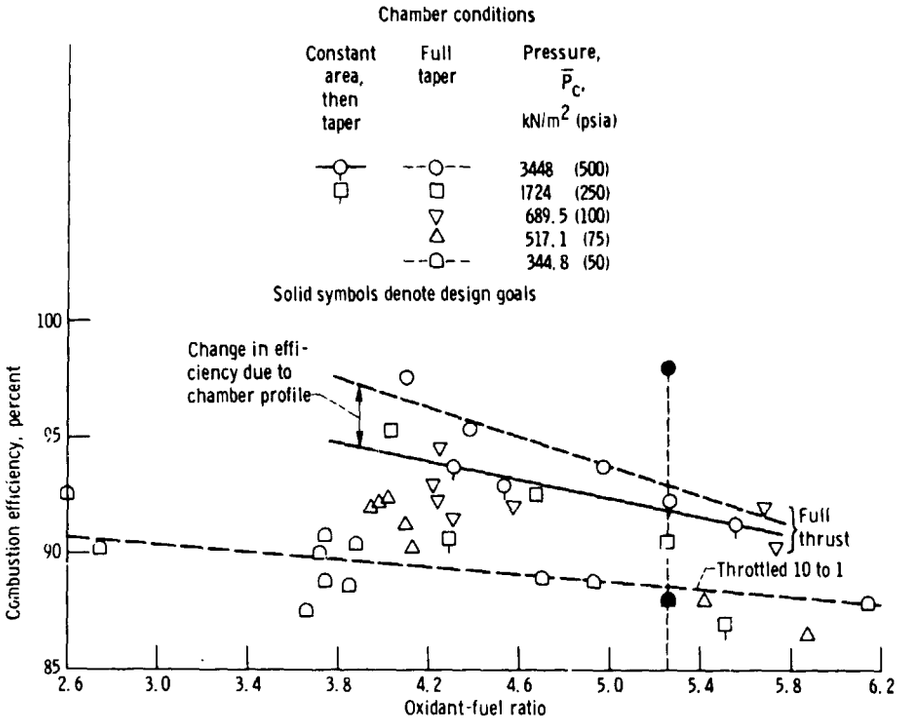

Figure 10. - Combustion efficiency as function of oxidant-fuel ratio for various chamber pressures. Injector B; with constant flow areas and without hydraulic swirl for all elements.

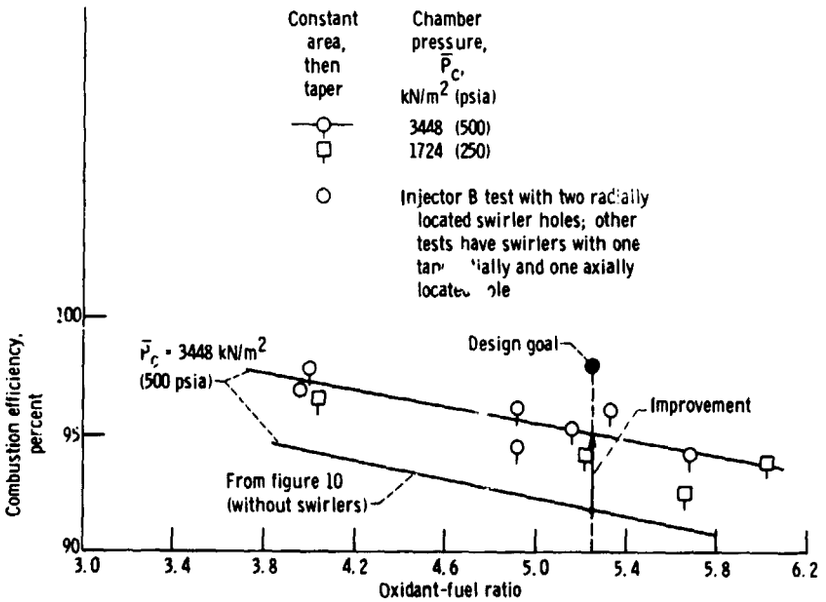

Figure 11. - Combustion efficiency as function of oxidant-fuel ratio at high chamber pressures. Injector C; effect of changing distribution of flow areas and adding hydraulic swirlers.

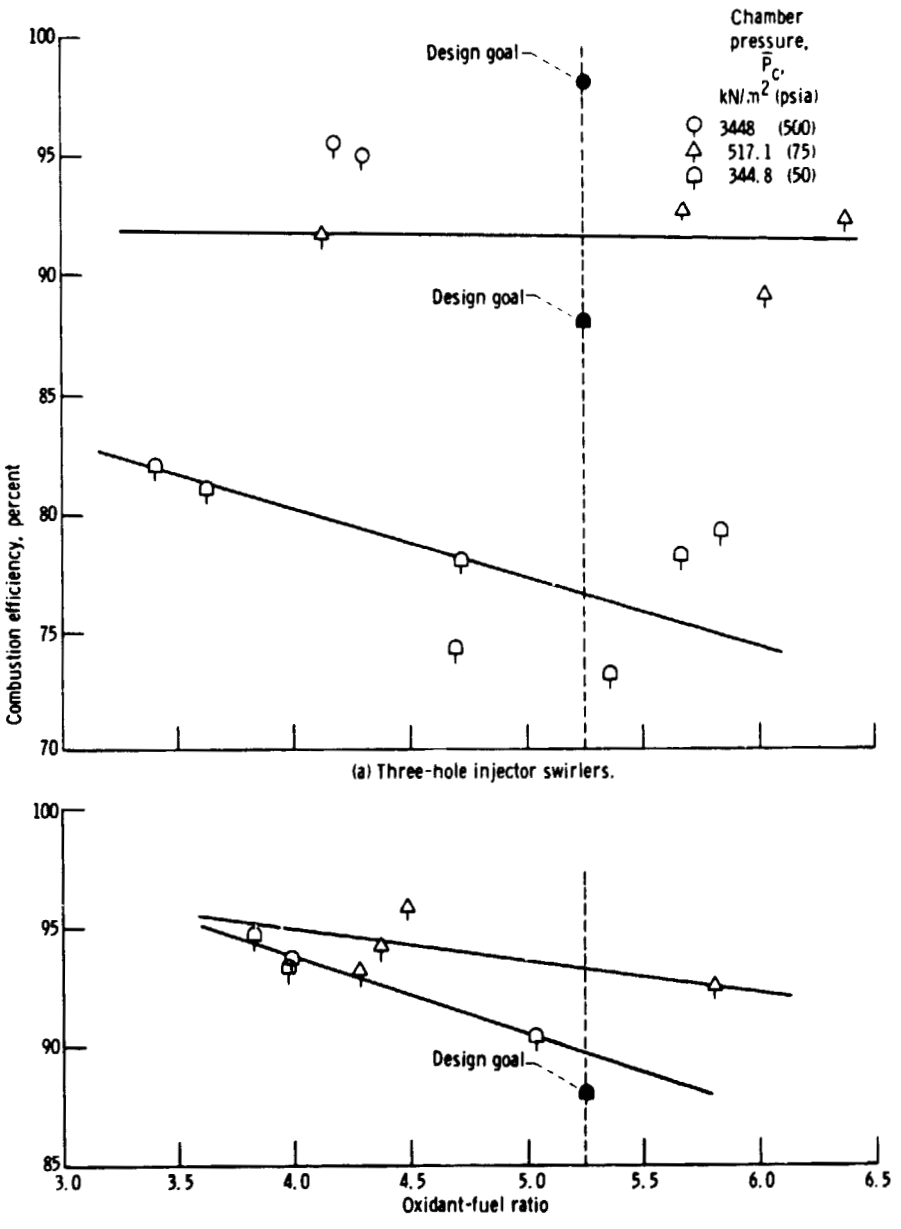

(a) Three-hole injector swirlers.

(b) No injector swirlers.

Figure 12. - Combustion efficiency as function of oxidant-fuel ratio for various chamber pressures. Injector D - no annulus flare and 0.0010-meter (0.040-in.) recessed tubes. Chamber: constant area, then taper.

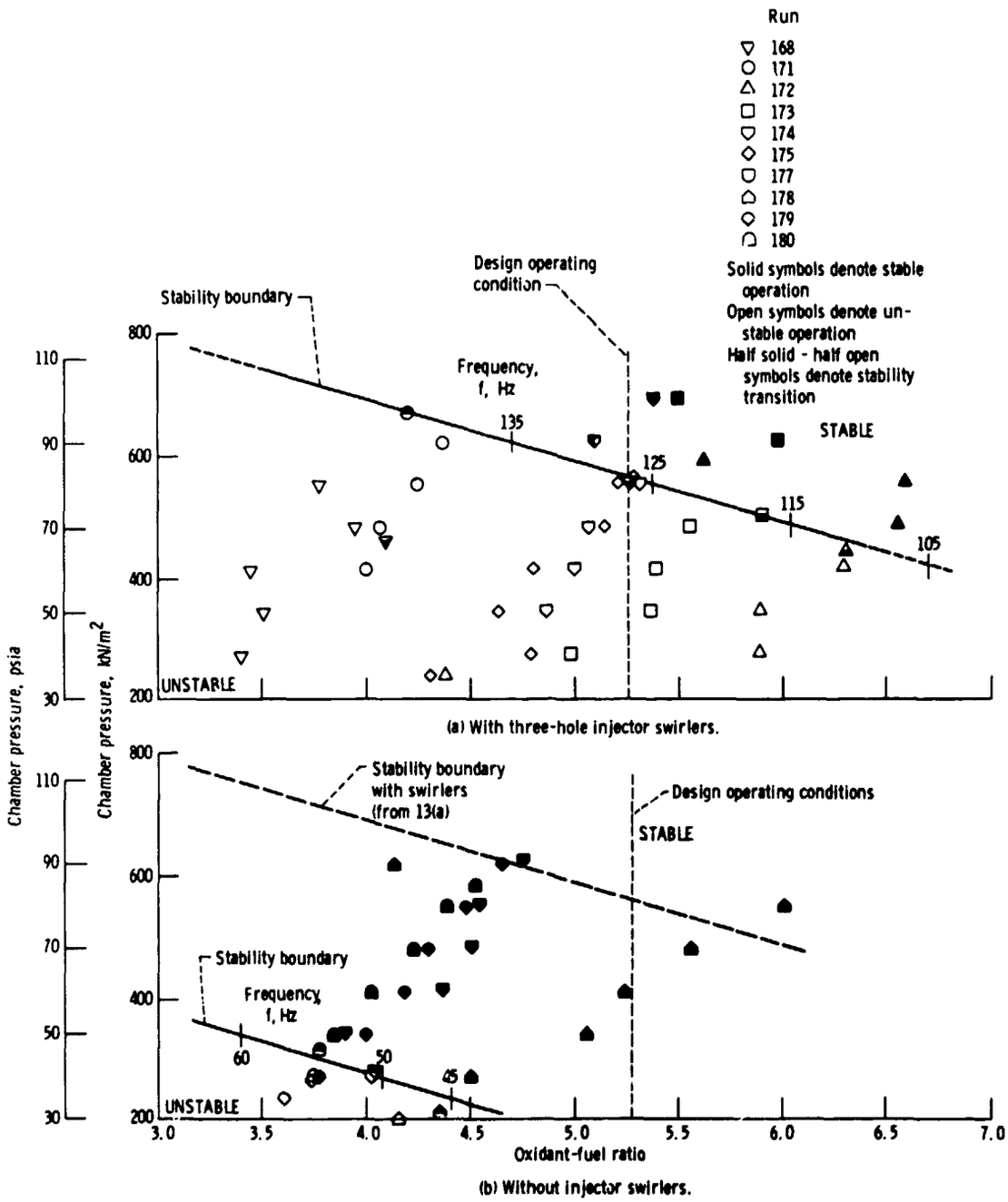

Figure 13. - Chamber pressure as function of oxidant-fuel ratio stability map for injector D.

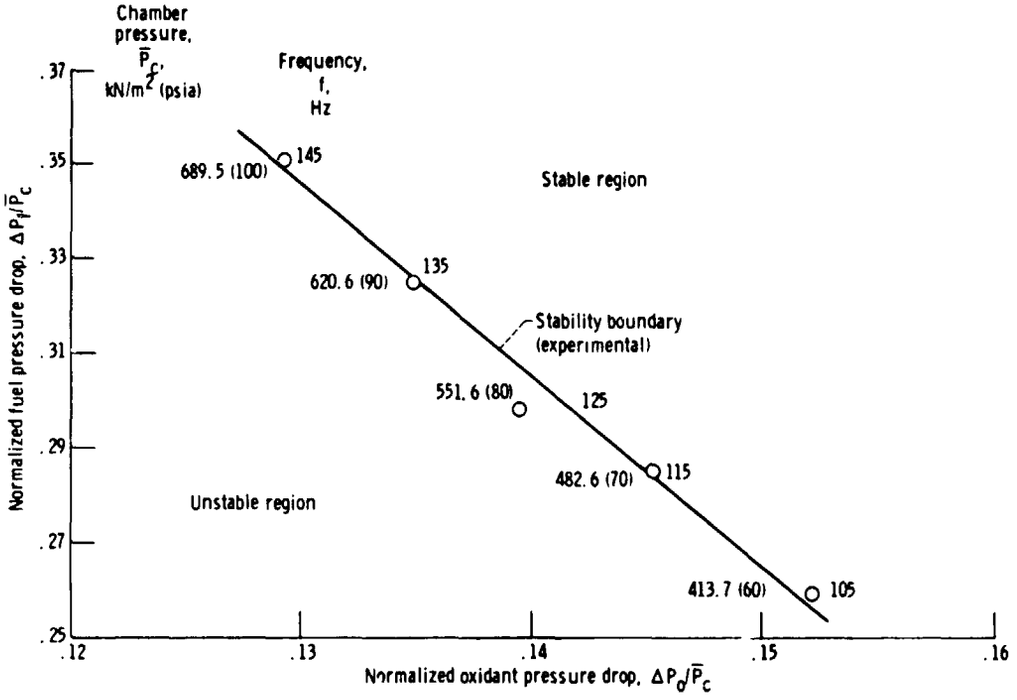

Figure 14. - Stability map for injector D with three-hole swirlers.

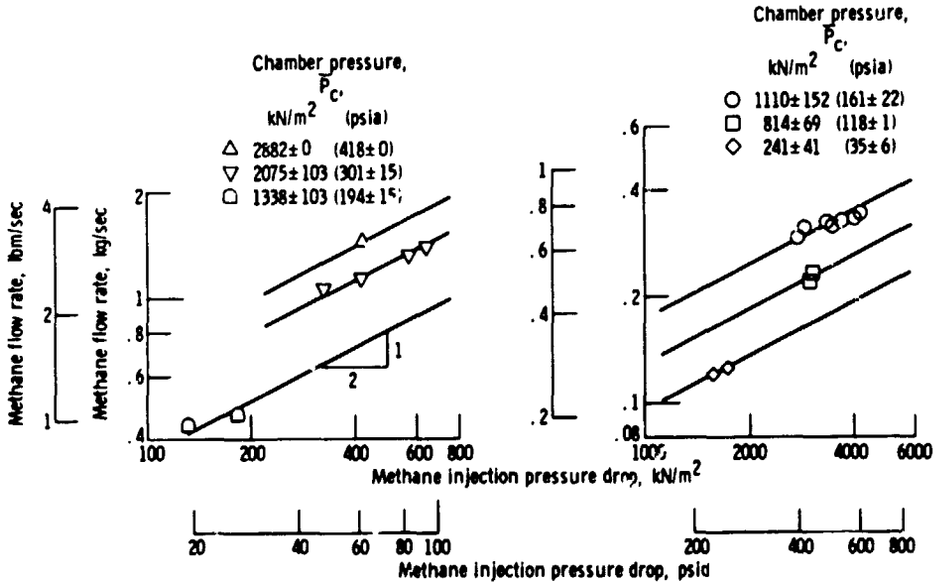

(a) Rigimesh I - used on injector A. Porosity: 24.78 cubic meters (875 ft^3) at pressure drop across faceplate, ΔP, 20.7 kilonewtons per square meter (3 psi) with air.

(b) Rigimesh II - used on injectors A, B, C, and D. Porosity: 8.5 cubic meters (300 ft^3) at pressure drop across faceplate, ΔP, 138 kilonewtons per square meter (20 psi) with air.

Figure 15. - Methane flow rate as function of methane injection pressure drop for two Rigimesh materials.

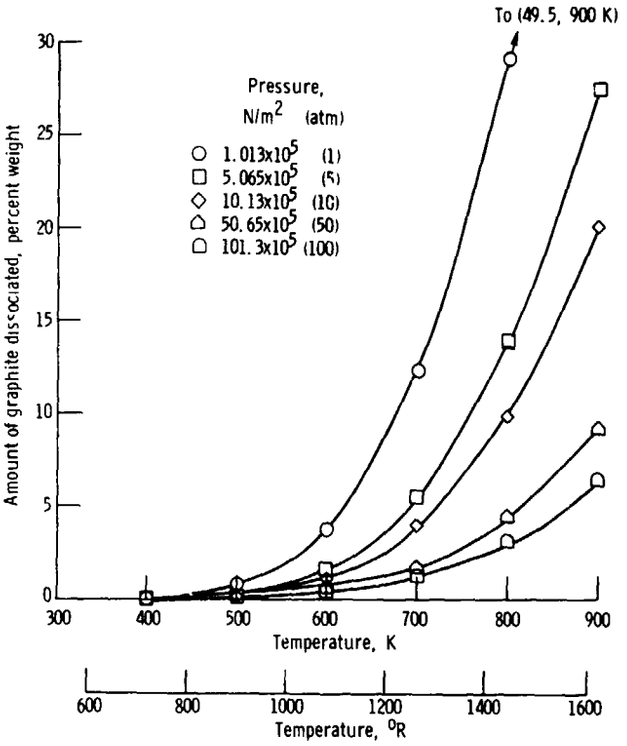

Figure 16. - Amount of graphite dissociated as function of temperature and pressure for high-temperature methane. Steady-state analysis; nonflowing fluid (based on chemical equilibrium program of ref. 11).

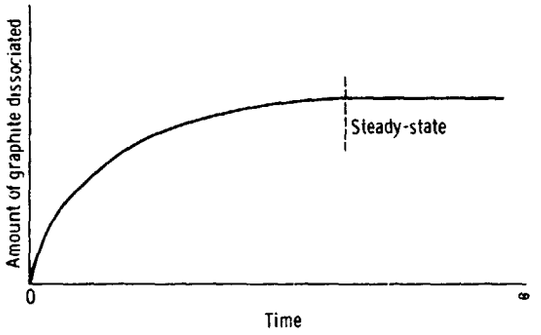

Figure 17. - Pseudo-plot of amount of graphite dissociated as function of time for high-temperature methane. Constant pressure and temperature.

NASA-Langley, 1974 E-7911